iJET EXPLORE International Journal of Engineering & Technology
CENTRE OF PROFESSIONAL RESEARCH PUBLICATIONS
ISSN 2049-3444

International Journal of Engineering and Technology Volume 2 No. 4, April, 2012

A Shunt Active Power Filter with Enhanced Performance Using ANN-Based Predictive and Adaptive Controllers

O.Arun kumar[1] S.Radha Krishna Reddy [2] JBV Subrahmanyam[3] PK Sahoo[4] Ch.Shashidhar[5]

[1,2] Electrical&Electronics Engineering Dept Holymary institute of technology&science,kesara, RR district, Hyderabad,AP,INDIA

[3,4,5] Electrical&Electronics Engineering Dept.,Bharat Institute of Engineering &Technology, mangalpally, ibrahimpatnam, RR district, Hyderabad,AP,INDIA 501 510

ABSTRACT

In this paper the aim of the study is to improve the dynamic performance of a shunt-type active power filter. The predictive and adaptive properties of artificial neural networks (ANNs) are used for fast estimation of the compensating current. The dynamics of the dc-link voltage is utilized in a predictive controller to generate the first estimate followed by convergence of the algorithm by an adaptive ANN based network. Weights in adaptive ANN are tuned to minimize the total harmonic distortion of the source current. Extensive simulations and experimentations confirm the validity of the proposed scheme for balanced and unbalanced loads for a three-phase three-wire system.

Keywords—*Adaptive ANN, current control, nonlinear load, shunt active power filter (APF), total harmonic distortion (THD),voltage source inverter.*

I. INTRODUCTION

Harmonic compensations have become increasingly important in power systems due to the widespread use of adjustable-speed drives, arc furnace, switched-mode power supply, uninterruptible power supply, etc. Harmonics not only increase the losses but also produce unwanted disturbance to the communication network, more voltage and/or current stress, etc. Different mitigation solutions, e.g., passive filter, active power line conditioner, and also hybrid filter, have been proposed and used [1]–[8]. Recent technological advancement of switching devices and availability of cheaper controlling devices,e.g., DSP-/field-programmable-gate array-based system, make active power line conditioner a natural choice to compensate for harmonics. Shunt-type active power filter (APF) is used to eliminate the current harmonics.

The dynamic performance of an APF is mainly dependent on how quickly and how accurately the harmonic components are extracted from the load current. Many harmonic extraction techniques are available, and their responses have been explored. Proposed techniques include traditional $d-q$ [2] and $p-q$ theory [3]–[5] based approaches and application of adaptive filters [6], wavelet [7], genetic algorithm (GA), artificial neural network (ANN), etc., for quick estimation of the compensating current [8].
A critical evaluation of such techniques is recently reported by the authors [8].

Recently, ANNs have attracted much attention in different applications, including the APF [9]–[20], [22]. Dash *et al.* [14] computed the Fourier coefficients of the signal by using *adaptive ANN*, and Chen and O'Connell [15] used an ANN that is trained with GA and back propagation. Lai *et al.* [16] used a Hopfield neural network for real-time computation of frequency and harmonic content of the signal. Improved performance has been observed compared to discrete Fourier transform, fast Fourier transform, or Kalman-filtering-based approaches. Tey *et al.* [17] reported a modified version of [10]. An additional PI controller is used to regulate the dc-link voltage. A full "neuromimetic" strategy involving several *adaptive ANNs* has been reported by Abdeslam *et al.* [18]. The controller can adapt for unbalance and change in working conditions. Lin [19] proposed an intelligent neural-network-based harmonic detection, which is first trained with enough data (1400 patterns). The working model could compute the harmonic components with only onehalf of the distorted wave. An *adaptive ANN* based harmonic compensation is reported by Singh *et al.* [20]. Weights are computed online by the LMS algorithm. Luo *et al.* [21] demonstrated a 200-kVA laboratory prototype for a combined system for harmonic suppression and reactive power compensation using an optimal nonlinear PI controller, whereas a two-stage recursive least square based *adaptive ANN* is reported by Chang *et al.* [22] for harmonic measurement.

Note that parallel developments on predictive control techniques are reported for power controllers. These are also applied to APF [23], [24]. The implementation of APF using power balance at the dc link is reported by Singh *et al.* [25]. The dc-link voltage has been used to find the peak magnitude of the supply current for self-

supporting dc bus. However, no detail analysis of the dynamics of the dc-link voltage is available.

This paper is an integration of predictive and adaptive control techniques for fast convergence and reduced computations. Two ANN-based controllers are used for such purpose. The predictive controller generates the first estimate of the compensating current quickly after the change in load is detected. The change in voltage across the capacitor is used for this purpose. This is followed by an *adaptive ANN*-based controller to fast converge to the steady value. This paper is organized in seven sections. Section II deals with the formulation of the problem. Section III investigates the dynamics of the dc-link voltage. Predicting algorithm is covered in Section IV. *Adaptive ANN*-based algorithm is presented in Section V. Section VI presents the simulation and experimental results. Section VII concludes the work.

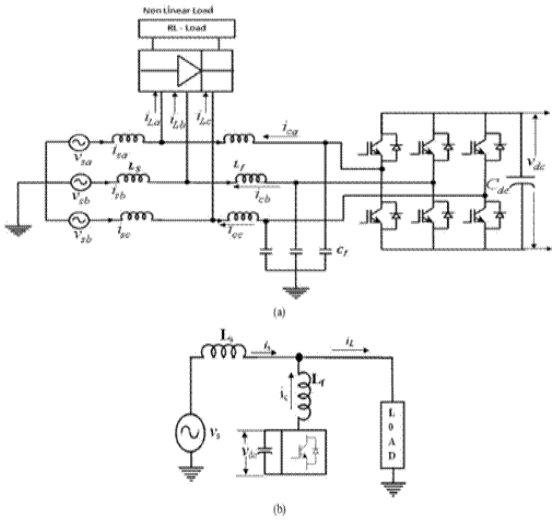

Fig. 1. (a) APF to compensate for a nonlinear load. (b) Single phase of shunt APF.

II. ESTIMATION OF CURRENT REFERENCE

Fig. 1(a) shows the APF compensating a nonlinear load. Fig. 1(b) shows the corresponding schematic diagram. A general expression for the load current [corresponding to Fig. 1(b)] is

$$i_L(t) = i_{\alpha 1} + i_{\beta 1} + i_h \quad (1)$$

The in-phase and quadrature components of the phase current at fundamental frequency are $i\alpha 1$ and $i\beta 1$, respectively. All other harmonics are included in ih. The per-phase source voltage and the corresponding in-phase component of the load current can be expressed as

$$v_{s(t)} = Vm \cos \omega t \quad (2)$$

$$i_{\alpha 1}(t) = I_{\alpha 1} \cos \omega t \quad (3)$$

Assuming that the APF will compensate for harmonic and reactive power, the compensating current becomes

$$i_c(t) = i_L(t) + i_{\alpha 1}(t) = i_L(t) - i_{\alpha 1} \cos \omega t \quad (4)$$

where $I\alpha 1$ is the peak magnitude of the in-phase current that the mains should supply and hence needs to be estimated. Once $I\alpha 1$ estimation is over, the reference current for the APF may easily be set as per (4). $iL(t)$ may be measured using current sensors. In the proposed scheme, estimation of $I\alpha 1$ is carried out by two stages.

A single-layer ANN-based algorithm first predicts the value of $I\alpha 1$ following which an *adaptive ANN*-based ANN is used for fast convergence. Note that the inverter also draws a small current ($is\alpha(t)$) to maintain the dc-link voltage.

III. CONTROL OF DC-LINK VOLTAGE IN APF

The dynamics of the dc-link voltage is an indirect measure of the performance of the APF. Whenever there is a change in the load, the voltage across the dc-link capacitor also undergoes a corresponding change. A controller is used to keep the voltage regulated at a desired value. In this section, a simple analysis of the dynamics of the dc-link voltage is first carried out. Parameters that govern the dynamics are identified, following which an algorithm is developed to estimate the compensating current of the APF.

To maintain the dc-bus voltage to a desired magnitude, the capacitor draws in-phase (i.e., in phase with the source voltage) current $is\alpha$. This is in addition to the compensating current ic. From the power balance equation

$$p_{dc} = c_{dc} v_{dc} \frac{dv_{dc}}{dt} \quad (5)$$

where $p$dc is the power required to maintain the voltage $v$dc across the dc link.

From the power balance equation

$$\sum_{i=a,b,c} v_{ci}(t) i_{ci}(t) - \sum_{i=a,b,c} R_f \left(i_{sci}^2(t) + i_{ci}^2(t) \right) - \frac{1}{2} \sum_{i=a,b,c} L_f \frac{d}{dt} \left(i_{sci}^2(t) + i_{ci}^2(t) \right) = i_{dc}(t) v_{dc}(t) = p_{dc} \quad (6)$$

where Rf and Lf are the resistance and inductance of the inductor that is connected in between the point of common coupling and the voltage source inverter. Note that $is\alpha$ supplies the system loss at the steady state and charges/discharges the capacitor during transient to maintain the dc-link voltage. Considering that "power" is a scalar quantity, (6) for a balanced three-phase system may be expressed as

$$3v_s(t)i_s(t) - 3R_f(i_{sa}^2(t) + i_c^2(t)) - \frac{3}{2}L_f\frac{d}{dt}(i_{sa}^2(t) + i_c^2(t)) = i_{dc}(t)v_{dc}(t) = p_{dc} \quad (7)$$

Applying small perturbations in *ic*, *isα*, *v*dc, and *vs*, around an operating point, the following new set of variables may be obtained:

$$i_c(t) = I_c + \Delta i_c \quad (8)$$

$$i_{sa}(t) = I_{sa} + \Delta i_{sa} \quad (9)$$

$$v_{dc}(t) = V_{dc} + \Delta v_{dc} \quad (10)$$

$$v_s(t) = V_s + \Delta v_s \quad (11)$$

where *Ic*, *Isα*, and *Vs* are rms and *V*dc is the dc value of the corresponding quantities at the operating point.

Again, in steady state

$$3V_sI_{sa} - 3R_f(I_{sa}^2 + I_c^2) = 0 \quad (12)$$

Substituting (8)–(12) in (7), the following equation is obtained

$$3(\Delta v_sI_{sa} + V_s\Delta i_{sa}) - 6R_f(I_{sa}\Delta i_{sa} + I_c\Delta i_c) - 3L_f\left(I_{sa}\frac{d\Delta i_{sa}}{dt} + I_c\frac{d\Delta i_c}{dt}\right) = C_{dc}V_{dc}\frac{d\Delta v_{dc}}{dt} \quad (13)$$

Converting the variables to *s*-domain and after rearranging, (13) may be expressed as

$$\Delta Vdc(s) = \frac{KG_1(s)G_3(s)G_2(s)}{1+KG_1(s)G_3(s)G_2(s)}\Delta V_{dc}^*(s) - \frac{G_2(s)G_3(s)}{1+KG_3(s)G_1(s)G_2(s)}\Delta Ic(s) + \frac{G_2(s)G_4(s)}{1+KG_3(s)G_2(s)G_4(s)}\Delta V_s(s) \quad (14)$$

where *K* is the small-signal gain. Detail derivation of (14) from (13) is available in the Appendix.

Equation (14) confirms that the ripple in the dc-link voltage depends on $\Delta V * \mathrm{dc}$, ΔIc, and ΔVs. In our present problem, the distortion in source voltage and reference dc-bus voltage is not considered. Therefore, (14) further modifies to

$$\Delta Vdc(s) = -\frac{G_2(s)G_3(s)}{1+KG_3(s)G_1(s)G_2(s)}\Delta Ic(s) \quad (15)$$

This explores the possibility of extracting an estimate of the compensating current from the change in *v*dc.
The gains of the PI controller used to regulate the dclink voltage are governed by the following two inequalities [26]

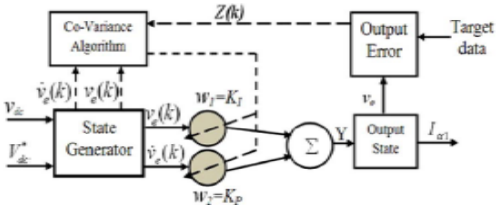

Fig. 2. Block diagram of ANN-based peak value predictor

$$Is < \frac{Cdcv_{dc}^*}{3KFLf} \quad (16)$$

$$Is \leq \frac{KPVs}{2RfKP + LfKI} \quad (17)$$

All the ac quantities in (16) and (17) are expressed as rms value. *Is*, $V * \mathrm{dc}$, and *Vs* are the source current, reference dc-link voltage, and source voltage, respectively. Equations (16) and (17) are used to generate an initial guess of *KP* and *KI* and also to set their limits.

IV. ANN-BASED FAST ESTIMATION OF COMPENSATING CURRENT

An ANN-based PI controller plays a dual role. It ensures faster reference generation and is also accountable for better regulation of dc-bus voltage. The structure of the system (i.e., ANN-tuned adaptive PI controller) is shown in Fig. 2. To reduce computational burden, a single-layer ANN structure is used. The input vector as expressed in (18) is fed to the state exchanger. In our scheme, error voltage and its gradient are chosen as the state of the system to ensure faster corrective action

$$u = [V_{dc}^* v_{dc}]^T \quad (18)$$

The task of the state generator block is to generate states *x*1 and *x*2 as follows

$$x_1 = v_e(k) \quad x_2 = \frac{\delta v_e}{\delta k} \quad (19)$$

where $ve(k) = V * \mathrm{dc} - v\mathrm{dc}(k)$. The output error $z(k)$ is represented as

$$z(k) = v_0(k) - v_0(k-1) \quad (20)$$

The output $vo(k)$ is fed to output state to estimate $I\alpha 1$.

Neuron cell generates controlling signal through interrelated gathering [27], [28] as

$$u(k) = u(k-1) + \sum_{i=1}^{2} w_i(k)x_i(k) \quad (21)$$

where *wi* is the weight of the system.

Here, a neuron is trained by Hebb's rule [27], [28]. Therefore, the change of weight of the neuron cell at *k*th instant may be represented as:

$$w_i(k+1) = (1-c)w_i(k) + \eta r_i(k) \quad (22)$$

$$r_i(k) = z(k)u(k)x_i(k) \quad (23)$$

where *ri* is the progressive signal, η is Hebb's studying ratio (learning rate), and "*c*" is a constant. Substituting (22) and (23) in (21), the following equation may be obtained

$$\Delta w_i(k) = w_i(k+1) - w_i(k) = -c\left[w_i(k) - \frac{\eta z(k)u(k)x_i(k)}{c}\right] \quad (24)$$

$\Delta wi(k)$ is the change of weight at *k*th step. Weights of the neuron are tuned according to Hebb's assumption. Hebb's assumption is popularly known as the covariance algorithm

$$\Delta w_i(k) = F_i(y_1(k)x_i(k)) \quad (25)$$

where $Fi(*)$ is a function of both postsynaptic and presynaptic signals and *y*1 is the output of the individual neuron. If $Fi(*)$ is differentiable, then $\delta Fi/\delta wi$ may be represented as:

$$\frac{\delta F_i}{\delta w_i} = w_i(k) - \frac{\eta}{c}z(k)u(k)x_i(k) \quad (26)$$

From (26), the change of weight in *k*th sample may be expressed as:

$$\Delta w_i(k) = -c\frac{\delta F_i(k)}{\delta w_i(k)} \quad (27)$$

Thus, by adjusting the values of $wi(k)$, *KP* and *KI* are tuned. The weights $wi(k)$ are searched according to the negative slope of function $Fi(*)$. Equations (26) and (27) are used to tune the parameter used in (28) and (29). Finally, for the PI controller, the weights are represented by:

$$w_1(k+1) = w_1(k) + \eta I^2(k)x_1(k) \quad (28)$$

$$w_2(k+1) = w_2(k) + \eta p^2(k)x_2(k) \quad (29)$$

Whenever the ANN is initiated, it starts with a set of controller gains to generate the first estimate of the compensating current. These initial values of controller parameters are set by offline training of the ANN. The controller parameters are then adjusted following (28) and (29) to regulate the dc-link voltage.

V. ADAPTIVE CURRENT DETECTION TECHNIQUE

The ANN in Section IV provides an initial guess for any change in system dynamics. To generate more accurate reference for APF, load current samples are fed to the *adaptive ANN*-based network shown in Fig. 3. *Adaptive ANN* is designed to minimize the total harmonic distortion (THD) of source current. Uncompensated source current sample $s(k)$ may be represented as

$$s(k) = I_{\alpha 1}\cos wkt_s + I_{\beta 1}\sin(wkt_s) + \sum_{n=2}^{R}(I_n \cos nwkt_s + \emptyset_n) \quad (30)$$

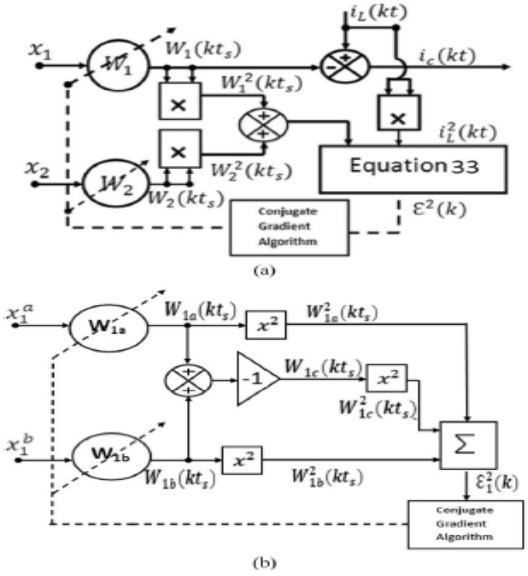

Fig. 3. (a) Adaptive ANN-based harmonic extraction for a three-phase balanced network. (b) Adaptive ANN-based harmonic extraction for a three-phase unbalanced network.

where *ts* is the step size in discrete domain. The square of error terms for *k*th sample may be expressed as:

$$\varepsilon^2(k) = \left[\frac{[s^2(k) - 2s(k)a(k)]}{a^2(k)} + 1\right] \quad (31)$$

Where

$$a^2(k) = I_{\alpha 1}^2(k)\cos^2(wkt_s) + I_{\beta 1}^2(k)\sin^2(wkt_s) \quad (32)$$

Equation (31) may also be represented as

$$\varepsilon^2(k) = \left[\frac{[s^2(k) - 2s(k)[x^T(k)\bar{a}(k)\bar{a}^T(k)x(k)]}{x^T(k)\bar{a}(k)\bar{a}^T(k)x(k)} + 1\right] \quad (33)$$

where the vector

$$\bar{a}(k) = \left[I_{\alpha 1}(k), I_{\beta 1}(k)\right] \quad (34)$$

and the input vector

$$X(k) = [\cos wkt_s, \sin wkt_s]^T \quad (35)$$

Equation (33) is further modified to fit in terms of a quadratic equation as:

$$A\{(\bar{a}^T(k)x(k))^T(\bar{a}^T(k)x(k))\} - B[\bar{a}^T(k)x(k)] + c = 0 \quad (36)$$

where $A = (1 - \varepsilon 2(k))$, $B = 2s(k)$, and $C = s2(k)$.

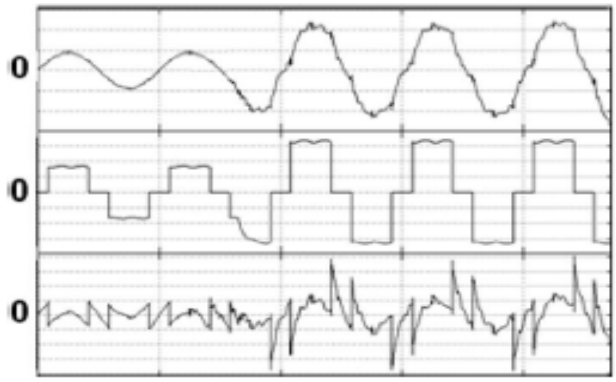

Fig. 4. Performance of the APF with predictive ANN (simulation results)

Top waveform: Source current of phase A (scale: 5 A/div). Middle waveform: Load current of phase A (scale: 5 A/div). Bottom waveform: Compensating current of phase A (scale: 5 A/div). Time scale: 20 ms/div.

Equation (36) is minimized by *conjugate gradient* (CG) method [27]–[29].

Thus, the error function (i.e., THD) is minimized to calculate the in-phase component of the fundamental load current. The compensating current is then calculated according to (4). Convergence of this method is faster than existing *adaptive ANN*-based schemes due to the use of less number of tuning blocks. The orthogonal relationship between the input vectors reduces the computational burden of the system.

Fig. 3(a) shows the details of current detection for a threephase balanced system, while Fig. 3(b) shows the same for an unbalanced (three-phase and three-wire) network. *W*1*a*, *W*1*b*, and *W*1*c* are the corresponding in-phase components of the current for phase-a, phase-b and phase-c, respectively.

VI. SIMULATION AND EXPERIMENTAL RESULTS

Simulations have been conducted for balanced and unbalanced loads using SIMULINK for different controller configurations. Switching frequency of the inverter is set at 10 kHz, and the dead time of the inverter is set at 2 μs. An experimental prototype is also made in the laboratory to verify the performance of the proposed predictive and adaptive ANN-based reference generation technique for APF. A current-controlled inverter using insulated-gate bipolar transistors, which is available in the laboratory, is used for this purpose. A 110-V 50-Hz mains supplying a load of 3 kVA is considered. A dSPACE-1104- based software, as well as hardware environment, is created where the ANN routine is written in MATLAB/C/C++ code. The whole system is built in SIMULINK where the ANN routine is called whenever necessary.

First, simulation study is made for the case with only predictive algorithm. Fig. 4 shows the waveform for balanced and nonlinear load. A diode bridge feeding a highly inductive network is treated as the nonlinear load. The figure shows the source, load, and compensating currents in top-to-bottom order. Load change has occurred at 40 ms. The initial estimate of the source current is extracted from the dip in capacitor voltage (according to the algorithm explained in Section IV). Fig. 5 shows the corresponding results from the experimentation. The THD of the source current in simulation and experimental results are 14.2% and 14.9%, respectively.

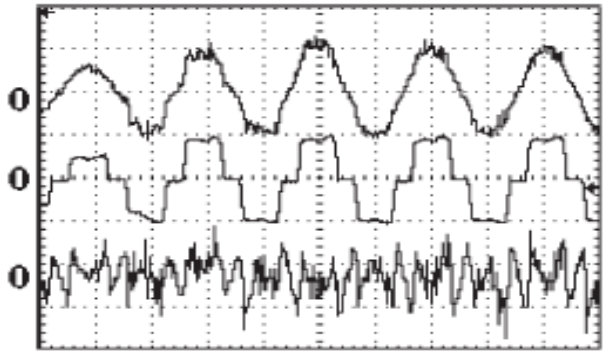

Fig. 5. Performance of the APF with predictive ANN (experimental results)

Top waveform: Source current of phase A (scale: 20 A/div). Bottom waveform: Load current of phase A (scale: 20 A/div). Middle waveform: Compensating current of phase A (scale: 10 A/div). Time scale: 10 ms/div.

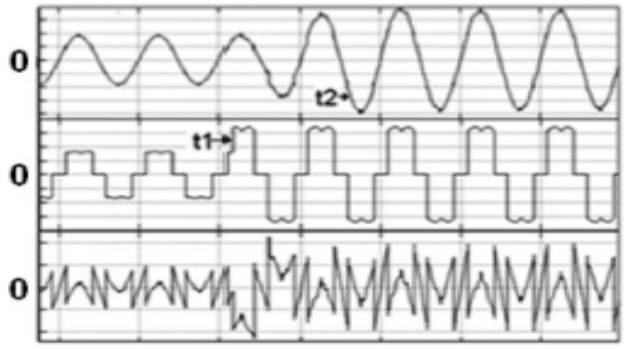

Fig. 6. Performance of the APF with *adaptive ANN* (simulation results)

Top waveform: Source current of phase A (scale: 5 A/div). Middle waveform: Load current of phase A (scale: 5 A/div). Bottom waveform: Compensating current of phase A (scale: 5 A/div). Time Scale: 20 ms/div.

Although a quick estimate helped, the waveform quality is poor due to the lack of any corrective mechanism in the system. The experimental and simulation results matched.

Next, the adaptive algorithm is tried. Simulation and experimentation are conducted to check the performance of the system for a step change in load. Balanced three-phase nonlinear load is considered similar to the case with predictive algorithm. Figs. 6 and 7 show the corresponding simulation and experimental results. In the figures, t1 shows the time when the load is changed, and t2 shows the instant when the system has reached steady state. The controller took 36 and 42 ms to converge in simulations and experimentation, respectively.

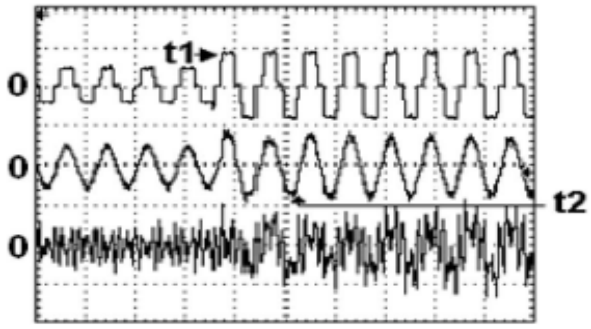

Fig. 7. Performance of the APF with *adaptive ANN* (experimental results). (a) Load current of phase A (scale: 20 A/div). (b) Source current of phase A (scale: 20 A/div). (c) Compensating current of phase A (scale: 20 A/div). Time scale: 20 ms/div.

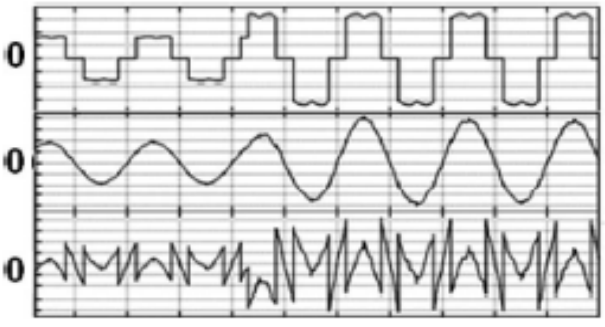

Fig. 8. Performance of the APF with predictive and adaptive controllers (simulation results). (a) Load current of phase A (scale: 5 A/div). (b) Source current of phase A (scale: 20 A/div). (c) Compensating current of phase A (scale: 5 A/div). Time scale: 10 ms/div.

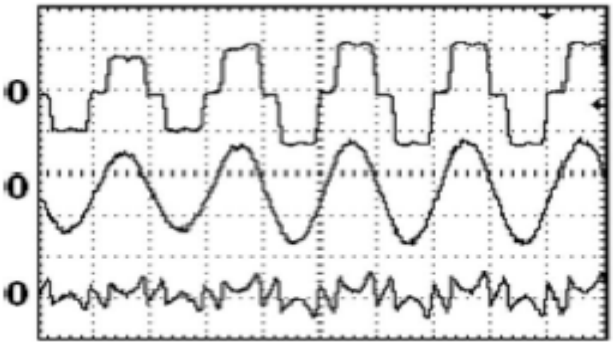

Fig. 9. Performance of the APF with predictive and adaptive controllers (experimental results). (a) Load current of phase A (scale: 20 A/div). (b) Source current of phase A (scale: 20 A/div). (c) Compensating current of phase A (scale: 10 A/div). Time scale: 10 ms/div.

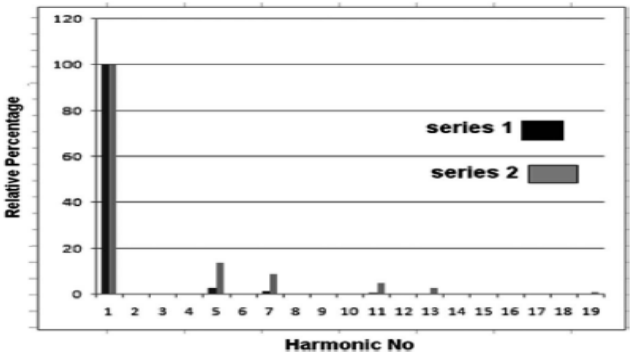

Fig. 10. Harmonic spectra for the compensated source current (series 1) and load current (series 2) of Fig. 9. Note that the system took more time to converge as there is no predictive mechanism; however, the waveform quality is much better with the THDs of 5.2% and 5.5% for the simulation and experimental results, respectively.

Now, to have the advantage of predictive and adaptive controllers, the system is run with both the algorithms. Figs. 8 and 9 show the situation with both the predictive and adaptive controllers in operation. The results have confirmed very satisfactory performance in terms of waveform quality and response time. The THDs for both the simulation and experimental results remain less than 5%. Fig. 10 shows the individual harmonic contents (particularly the lower order harmonics) for both compensated and uncompensated source currents. The THD of the compensated source current is found to be 4.6%. Some experiments are also conducted for unbalanced nonlinear load. A severe unbalance such as single phasing is considered as shown in Fig. 11.

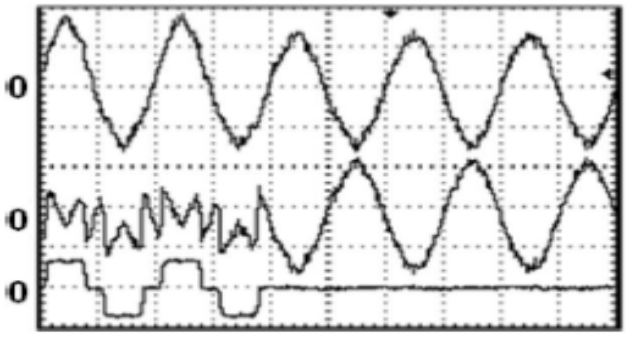

Fig. 11. Performance of the APF in the case of single phasing (experimental results). (a) Source current of phase A (scale: 10 A/div). (b) Compensating current of phase A (scale: 10 A/div). (c) Load current of phase A (scale: 20 A/div). Time scale: 10 ms/div.

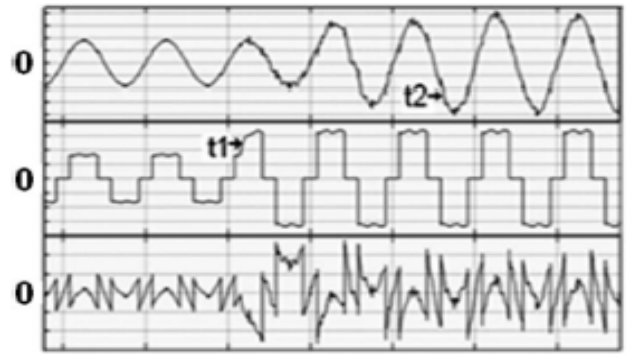

The controller is found to operate satisfactorily. Finally, the performance of the proposed controller is compared with that of a traditional controller (such as synchronous reference frame based). The synchronous reference frame controller is simulated (using the cutoff frequency of the low-pass filter as 10 Hz). Fig. 12 shows corresponding dynamic performance. The source current, load current, and compensating current are shown in top-to-bottom order. The controller took 52 s to converge, whereas the proposed controller with predictive and adaptive algorithm converged within less than one-quarter of a cycle with acceptable current quality.

VII. CONCLUSION

An integration of predictive and adaptive ANN-based controller for a shunt-type APF has been presented in this paper to improve the convergence and reduce the computational requirement. The predictive algorithm is derived from an ANN based PI controller used to regulate the dc-link voltage in the APF. This is followed by an *adaptive ANN*-based THD minimization technique. *Adaptive ANN* is trained by CG method to minimize THD. Use of only two weights and two input vectors makes the convergence very fast. The system is extensively simulated in MATLAB/SIMULINK. An experimental prototype is produced in the laboratory using dSPACE1104. The results from experiments match well with the simulation, confirming the usefulness of the proposed technique.

REFERENCES

[1] B. Singh, K. Al-Haddad, and A. Chandra, "A review of active power filters for power quality improvements," *IEEE Trans. Ind. Electron.*, vol. 46, no. 5, pp. 960–971, Oct. 1999.

[2] S. Bhattacharya, T. M. Frank, D. M. Divan, and B. Banerjee, "Active filter system implementation," *IEEE Ind. Appl. Mag.*, vol. 4, no. 5, pp. 47–63, Sep./Oct. 1998.

[3] H. Akagi, Y. Kanazawa, and A. Nabae, "Instantaneous reactive power compensators comprising switching devices without energy storage= components," *IEEE Trans. Ind. Appl.*, vol. IA-20, no. 3, pp. 625–630, May 1984.

[4] F. Z. Peng, G.W. Ott, Jr., and D. J. Adams, "Harmonic and reactive power compensation based on the generalized instantaneous reactive power theory for three phase four wire system," *IEEE Trans. Power Electron.*, vol. 13, no. 6, pp. 1174 1181, Nov. 1998.

[5] R. S. Herrera and P. Salmeron, "Instantaneous reactive power theory: A reference in the nonlinear loads compensation," *IEEE Trans. Ind. Electron.*, vol. 56, no. 6, pp. 2015–2022, Jun. 2009.

[6] H. Karimi, M. Karimi-Ghartemani, and M. R. Iravani, "An adaptive filter for synchronous extraction of harmonics and distortions," *IEEE Trans. Power Del.*, vol. 18, no. 4, pp. 1350 1356, Oct. 2003.

[7] M. Forghani and S. Afsharnia, "Online wavelet transform based control strategy for UPQC control system," *IEEE Trans. Power Del.*, vol. 22, no. 1, pp. 481–491, Jan. 2007.

[8] A. Bhattacharya, C. Chakraborty, and S. Bhattacharya, "Current compensation in shunt type active power filters," *IEEE Ind. Electron. Mag.*, vol. 3, no. 3, pp. 38–49, Sep. 2009.

[9] A. Hamadi, S. Rahmani, and K. Al-Haddad, "A hybrid passive filter configuration for VAR control and harmonic compensation," *IEEE Trans. Ind. Electron.*, vol. 57, no. 7, pp. 2419–2434, Jul. 2010.

[10] B. Widrow and M. A. Lehr, "30 years of adaptive neural networks: Perceptron, madaptive ANN and backpropagation," *Proc. IEEE*, vol. 78, no. 9, pp. 1415–1442, Sep. 1990.